

Adaptively Multi-view and Temporal Fusing Transformer for 3D Human Pose Estimation

Hui Shuai*, Lele Wu*, and Qingshan Liu, *Member, IEEE*

Abstract—In practical application, 3D Human Pose Estimation (HPE) is facing with several variable elements, involving the number of views, the length of the video sequence, and whether using camera calibration. To this end, we propose a unified framework named Multi-view and Temporal Fusing Transformer (MTF-Transformer) to adaptively handle varying view numbers and video length without calibration. MTF-Transformer consists of Feature Extractor, Multi-view Fusing Transformer (MFT), and Temporal Fusing Transformer (TFT). Feature Extractor estimates the 2D pose from each image and encodes the predicted coordinates and confidence into feature embedding for further 3D pose inference. It discards the image features and focuses on lifting the 2D pose into the 3D pose, making the subsequent modules computationally lightweight enough to handle videos. MFT fuses the features of a varying number of views with a relative-attention block. It adaptively measures the implicit relationship between each pair of views and reconstructs the features. TFT aggregates the features of the whole sequence and predicts 3D pose via a transformer, which is adaptive to the length of the video and takes full advantage of the temporal information. With these modules, MTF-Transformer handles different application scenes, varying from a monocular-single-image to multi-view-video, and the camera calibration is avoidable. We demonstrate quantitative and qualitative results on the Human3.6M, TotalCapture, and KTH Multiview Football II. Compared with state-of-the-art methods with camera parameters, experiments show that MTF-Transformer not only obtains comparable results but also generalizes well to dynamic capture with an arbitrary number of unseen views. Code is available in <https://github.com/lelexx/MTF-Transformer>.

Index Terms—3D human pose estimation, Multi-view Fusing Transformer, Temporal Fusing Transformer.

1 INTRODUCTION

THREE dimension pose estimation aims at estimating 3D joint locations of human body parts from images or videos. It plays a fundamental role in many applications, such as action recognition [1], [2], [3], [4], human body reconstruction [5], [6], [7], and robotics manipulation [8]. In recent years, deep learning-based 3D HPE has made considerable progress. In this paper, we will focus on deep learning-based methods.

In practice, several factors affect the pipeline of 3D HPE, involving the number of views, the length of the video sequence, and whether using camera calibration. The combination of these factors derives many frameworks (shown in Fig. 1) that handle different application scenes. For clearly showcasing diverse frameworks, we first divide 3D HPE into monocular and multi-view methods according to the number of views, then further consider other factors for a more specific description.

In the monocular scene, most works [9], [10], [11], [12] estimate human body structure from a static image with elaborate networks. This paradigm is convenient since a single image is easy to obtain, and the network is easy to construct. Nevertheless, the information in a single image is far from sufficient considering the occlusion and depth ambiguity. For compensation, some works [13], [14], [15], [16], [17] utilize temporal information from video sequences. Sequential variation in the video is conducive to reveal the structure of the human body. However, continuous images contain more consistent information rather than complementary clues. In a word, monocular 3D HPE is easy to implement, but it

3D Pose Estimation(single-person)			
monocular		multi-view	
single image	video sequence	single image	video sequence
<ul style="list-style-type: none"> ● SemGCN[48] ● FCN[25] ● Cascaded[19] ● GOR[34] ● SRNeT[44] ● MDN[17] ● Skeletal-GNN[45] 	<ul style="list-style-type: none"> ● ViewPose3D[30] ● OAN[4] ● SRNeT[44] ● Motion-guided[42] ● PoseFormer[49] ● Skeletal-GNN[45] 	<p>w calibration</p> <ul style="list-style-type: none"> ● Epipolar Transformer[7] ● CrossView[32] ● Learnable[10] ● AdaFuse[47] 	<ul style="list-style-type: none"> ● FLEX[6]
		<p>w/o calibration</p> <ul style="list-style-type: none"> ● FLEX[6] ● DeepFuse[8] 	

Fig. 1. We classify frameworks of 3D HPE into monocular and multi-view methods according to the number of views. They are further divided into single-image based and video based methods. In multi-view methods, single-image based methods consists of methods with camera calibration and without calibration.

remains an ill-posed problem.

Recently, prevalent works [18], [19], [20] tend to utilize multi-view geometric constrains. Most existing multi-view methods aggregate features from different views via projective geometry, depending on calibrated parameters. Camera parameters incorporate solid prior knowledge into the network but are difficult to accurately calibrated in dynamic capture. To this end, some other works [21] attempt to fuse multi-view features without calibration, but they have strict requirements on camera configuration and the number of views. In addition, massive computation in the geometric space hinders multi-view methods to deal with video sequences. Overall, most existing multi-view methods are more accurate, but camera calibration and computation overhead limit their application scenes.

- Hui Shuai, Lele Wu, and Qingshan Liu are with Nanjing University of Information Science and Technology, 210044
E-mail: huishuai13@nuist.com, llwu@nuist.edu.cn, qslu@nuist.edu.cn
- Hui Shuai and Lele Wu equally contributed on the work. Qingshan Liu is the corresponding author.

Manuscript received April 19, 2005; revised August 26, 2015.

Each above-mentioned framework targets one or a few particular combinations of those factors and is not compatible with others, limiting the flexibility of the 3D HPE algorithm. Thus, it is essential to develop a unified framework that can adaptively handle all the factors. Specifically, a unified framework needs to be compatible with monocular to multi-view, single-image to video 3D HPE: (1) The framework should fuse features from an arbitrary number of views without customized retraining. (2) It is required to integrate multi-view features in uncalibrated scenes since synchronous camera calibration in dynamic capture is unrealistic. (3) It should adaptively fuse temporal features lying in the varying-length videos, and be compatible with a single image. (4) It should be lightweight enough to handle multi-view videos.

To satisfy these requirements, we propose a unified framework to deal with variable multi-view sequences without calibration, named Multi-view and Temporal Fusing Transformer (MTF-Transformer). MTF-Transformer consists of Feature extractor, Multi-view Fusion Transformer (MFT), and Temporal Fusion Transformer (TFT). In the Feature Extractor, a pre-trained 2D detector predicts 2D pose of each frame first. Then, coordinates and confidence are encoded into a vector via a Confidence Attentive Aggregation (CAA) block, discarding the image features. It makes the subsequent modules lightweight and focuses on lifting the 2D pose into the 3D pose. The Multi-view Fusing Transformer (MFT) fuses the features of multiple views into more informative ones. It integrates the relationship between the views into the procedure to calculate the key, query, and value in the relative-attention block, avoiding the need for camera calibration. Besides, the transformer can perceive the global relationship of all the tokens better [22]. In the Temporal Fusing Transformer (TFT), we employ a conventional transformer to capture temporal information. It is worth mention that, to make the MTF-Transformer adaptive to the input of an arbitrary number of views and length of sequences, we design a random mask mechanism in both MFT and TFT, referring to the dropout mechanism [23] in CNNs.

We evaluate our method on Human3.6M [24], TotalCapture [25], and KTH Multiview Football II [26] quantitatively and qualitatively. We also conduct detailed ablation study experiments to verify the effectiveness of each module. Experiment results demonstrate that MTF-Transformer outperforms camera parameter-free methods by a large margin. Beside, MTF-Transformer can be directly applied to the scene with different setting from the training stage, bridging the generalization gap significantly. In short, our contributions are:

- We proposed a unified framework (MTF-Transformer) for 3D HPE. It is adaptive to scenes with a video of arbitrary length and from arbitrary views without retraining.
- We design a novel Multi-view Fusing Transformer (MFT), where the relationship between views is integrated into the relative-attention block. MFT reconstructs the features from multiple views according to estimated implicit relationship, avoiding the need for camera calibration.
- We introduce the random mask mechanism into MFT and Temporal Fusing Transformer (TFT) to make them robust to variable view number and video length.
- Not only does our model outperforms camera parameter-free models by a large margin, but also has better generalization ability to handle diverse application scenes.

2 RELATED WORK

In this section, we discuss the methods based on deep neural networks for single-person 3D pose estimation. We divide them into monocular pose estimation and multi-view pose estimation.

2.1 Monocular Pose Estimation

Monocular pose estimation predicts the 3D pose of the person from a single image. According to different modalities, it further develops into two streams: single-frame-based methods and video-based methods.

Single-frame-based methods: With the excellent feature extraction capacity of deep neural networks, many approaches [5], [9], [27], [28], [29], [30], [31], [32] directly map pixel intensities to 3D poses from a single image. Li et al. [30] apply CNNs to jointly estimate 3D poses and detect body parts via a multi-task framework. However, training deep models directly from images requires expensive computation resources. Differently, a computationally lightweight method [9] decouples the task into two independent stages where they firstly predict 2D joint locations in image space and then lift them to 3D space. Thus, we encode each frame into a 1D feature vector to reduce computational overhead. Although a single image is easy to obtain and the network is easy to construct, the information in a single image is far from enough due to occlusion and depth blur.

Video-based methods: To obtain smoother 3D poses, more works [13], [14], [15], [33], [34] pay attention to temporal information in monocular video clips. Pavllo et al. [13] transform a sequence of 2D poses through temporal convolutions and make computational complexity independent of key-point spatial resolution. Cai et al. propose a graph-based method to incorporate spatial dependencies and temporal consistences [14]. Wang et al. [15] propose a novel objective function to explicitly involve motion modeling in learning. These methods are not compatible with static scenes and dynamic scenes. In addition, video sequences lack complementary information and cannot provide sufficient geometric constraints.

The 3D pose estimation in monocular scenes is easy to implement but it remains an ill-posed problem owing to the occlusion and depth ambiguity.

2.2 Multi-view Pose Estimation

To tackle the problems of occlusion and depth ambiguity in monocular 3D HPE, multi-view methods [18], [19], [35], [36], [37] exploit geometric information from multiple views to infer 3D pose. Most of them utilize intrinsic and extrinsic camera parameters to fuse 2D features from different views, and only a few works do not require camera parameters.

He et al. [18] propose the epipolar transformer that relies on camera calibration to aggregate features on epipolar lines between different views. As a dependent on camera parameters, the model can not handle the scenes of different camera configurations. Isakov et al. [19] utilize volumetric grids to fuse features from different views camera parameters and regress root-centered 3D pose through a learnable 3D CNN. Despite predicting 3D poses reliably, volumetric approaches are computationally demanding. Huang et al. [21] propose a new vision-IMU data fusion technique that does not need camera parameters but has strict requirements on camera configuration and the number of views. Gordon et al. [38] introduce a camera-parameter-free multi-view motion reconstruction algorithm to predict joint angles and bone lengths that

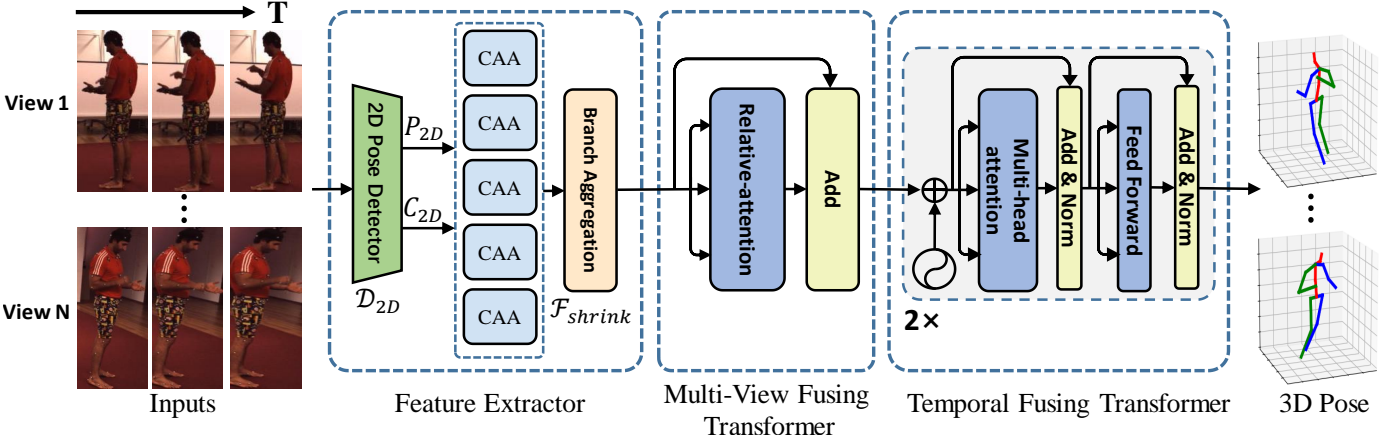


Fig. 2. Architecture of MTF-Transformer. It consists of three successive modules: Feature Extractor, Multi-view Fusing Transformer (MFT), and Temporal Fusing Transformer (TFT). Feature Extractor predicts 2D pose (P_{2D} and C_{2D}) first, and then encodes 2D pose into feature vector for each frame. MFT measures the implicit relationship between each pair of views and reconstructs the feature of each view according to the relationship. TFT aggregates the temporal information of the whole sequence and predicts the 3D pose.

are invariant to the camera position rather than directly predicting 3D positions. However, it is complicated and still cannot achieve good performance in the scenes with a single or a small number of views.

Multi-view pose estimation methods are more accurate owing to the effective feature fusing via projective geometry. However, another side of the coin is that these methods rely on the restricted camera configuration explicitly or implicitly, limiting their application scene.

Each method, in both monocular and multi-view methods, has its advantage and disadvantage and targets particular application scenes. Different from these methods, we attempt to propose a unified network that can predict robust 3D pose in all the application scenes, adapting to the view number and video length and avoiding camera calibration.

3 METHOD

The unified framework is supposed to adaptively handle features from an arbitrary number of views and arbitrary length of sequence without camera calibration. As shown in Fig. 2, the basic idea of the framework is to embed 2D detections into vector first, then fuse multi-view features, finally aggregate temporal clues to predict 3D joints. This framework consists of Feature Extractor, Multi-view Fusing Transformer, and Temporal Fusing Transformer.

3.1 Feature Extractor

Feature Extractor uses a pre-trained 2D pose detector (e.g., CPN [39]) to obtain 2D predictions, and then maps them into 1D feature vectors through a feature embedding module.

Taking multi-view sequences $\mathcal{I} = \{\mathbf{I}_i\}_{i=1}^{N \times T}$ with N views and T frames as input, each frame is a image $\mathbf{I} \in \mathbb{R}^{W \times H \times 3}$ with the size of $W \times H$. As the following operations are conducted on each frame, we will omit N and T for simplicity. For each frame, Feature Extractor first uses a pre-trained 2D pose detector \mathcal{D}_{2D} to infer the 2D prediction:

$$\mathbb{Z} = \mathcal{D}_{2D}(\mathbf{I}) \quad (1)$$

where $\mathbb{Z} = \{\mathbf{P}_{2D}, \mathbf{C}_{2D}\}$, $\mathbf{P}_{2D} = \{\mathbf{p}_j\}_{j=1}^J$ represents J 2D coordinates of the 2D pose and $\mathbf{C}_{2D} = \{\mathbf{c}_j\}_{j=1}^J$ represents the

confidence of these coordinates. Then a feature embedding module encodes the predicted 2D pose into a feature vector (as shown in Fig. 3).

The movements of the limbs and head are relatively independent, so we divide the human body joints into five partitions and deal with them in five parallel branches. The five partitions are the head, left and right arms, and left and right legs:

$$\mathbf{P}_{2D}^g = \{\mathbf{p}_k | k \in \mathbf{S}^g\} \quad (2)$$

$$\mathbf{C}_{2D}^g = \{\mathbf{c}_k | k \in \mathbf{S}^g\} \quad (3)$$

where g refers to the g -th partition, $g \in \{1, 2, 3, 4, 5\}$, $\mathbf{P}_{2D}^g, \mathbf{C}_{2D}^g$ are subset of $\mathbf{P}_{2D}, \mathbf{C}_{2D}$, $\mathbf{S}^g \subset \{1, 2, \dots, J\}$ represents the index set belongs to the g -th partition. For matrix multiplication, $\mathbf{P}_{2D}^g, \mathbf{C}_{2D}^g$ are reshaped into vectors that $\mathbf{p}_{2D}^g \in \mathbb{R}^{2J^g}$, $\mathbf{c}_{2D}^g \in \mathbb{R}^{J^g}$.

Since the 2D pose inferred from the pre-trained detector is unreliable due to motion blur and occlusion, simply fusing them may lead to unstable performance. Previous works, such as Gordon et al. [38], directly concatenate the 2D pose and confidence values together for aggregation but they ignore the effects of unreliable inputs on the features as the pose changes. In order to alleviate this issue, we utilize the confidence to modulate coordinates. Specifically, Confidence Attentive Aggregation (CAA) extracts local feature $\mathbf{f}^g \in \mathbb{R}^{C/2}$ for each part. It can be formulated as:

$$\bar{\mathbf{f}}^g = \mathcal{F}_p^g(\mathbf{p}_{2D}^g) \quad (4)$$

$$\mathbf{a}^g = \mathcal{F}_c^g(\mathbf{c}_{2D}^g) \quad (5)$$

$$\mathbf{f}^g = \mathcal{F}_{res}^g(\bar{\mathbf{f}}^g + \mathbf{a}^g \cdot \mathbf{p}_{2D}^g) \quad (6)$$

where \mathcal{F}_p^g is fully connected layer to map 2D coordinates \mathbf{p}_{2D}^g to initial feature vectors $\bar{\mathbf{f}}^g \in \mathbb{R}^{C/2}$, \mathcal{F}_c^g is another fully connected layer to learn a attention matrix $\mathbf{a}^g \in \mathbb{R}^{(C/2) \times 2J^g}$ from the confidence \mathbf{c}_{2D}^g . The third fully connected layers \mathcal{F}_{res}^g aggregates initial feature vectors $\bar{\mathbf{f}}^g$ with 2D coordinates \mathbf{p}_{2D}^g modulated by attention matrix \mathbf{a}^g . It consists of two res-blocks [9].

We further concatenate features of five partitions together and map them to a global feature $\mathbf{f} \in \mathbb{R}^C$. The procedure can be described as:

$$\mathbf{f} = \mathcal{F}_{shrink}(\text{Concat}(\mathbf{f}^1, \mathbf{f}^2, \mathbf{f}^3, \mathbf{f}^4, \mathbf{f}^5)) \quad (7)$$

where \mathcal{F}_{shrink} is another fully connected layer. It maps features from five branches to the final global feature of each frame. For

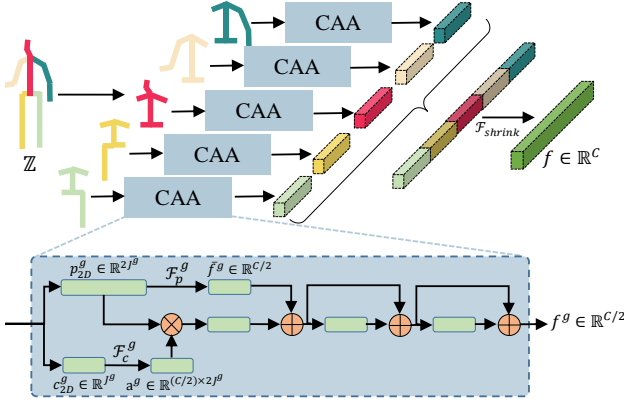


Fig. 3. Feature embedding module encodes the 2D prediction into a feature vector. It splits the 2D prediction into five partitions, and then use five branches to extract features. Finally, the features of five partitions are concatenated and mapped to a global feature f .

the input multi-view sequence \mathcal{I} with $N \times T$ frames, Feature Extractor extracts the feature $\mathbf{X} \in \mathbb{R}^{C \times N \times T}$ for the subsequent pipeline.

3.2 Multi-view Fusing Transformer

As mentioned above, our framework should measure the relationship between the features from an arbitrary number of views and utilize information about them. Recently, transformer model has made tremendous success in Natural Language Processing (NLP) and Computer Vision tasks [40]. It is characteristic with the ability to model dependencies in the input tokens regardless of their distance and enables immediate aggregation of global information [41]. Thus, transformer is suitable to measure the relationship between each pair of views and reconstruct the feature of each view according to the relationship. However, our purpose differs from conventional transformer in position encoding. In NLP and CV tasks, the absolute position is important for constructing semantic context. On the contrary, we only care about the relative relationship between each pair of views. Each view is equally important and we predict a 3D pose for each of them. So we modify the self-attention in transformer into Relative-Attention to bridge this gap.

3.2.1 Revisit Transformer and Self-attention

Transformer is a family of models consists of self-attention blocks, appending position encoding and mask block. In which, position encoding provides a unique coding for each input token. The mask block truncates some nonexistent connections base on prior knowledge. Self-attention operator transforms the input feature vectors $\mathcal{X} = \{\mathbf{x}_i\}_{i=1}^N$ into output feature vectors $\mathcal{Y} = \{\mathbf{y}_i\}_{i=1}^N$, one output feature vector \mathbf{y}_i is a weighted sum of all the input feature vectors. Typically, self-attention operators can be classified into scalar attention and vector attention [42].

The scalar dot-product attention can be formulated as follows:

$$\mathbf{y}_i = \sum_{\mathbf{x}_j \in \mathcal{X}} \rho(\varphi(\mathbf{x}_i)^\top \psi(\mathbf{x}_j) + \delta) \alpha(\mathbf{x}_j) \quad (8)$$

where φ , ψ , and α are pointwise feature transformations, such as linear projections or MLPs, $\varphi(\mathbf{x}_i)$, $\psi(\mathbf{x}_j)$, and $\alpha(\mathbf{x}_j)$ are called query, key, and value respectively. δ is a position encoding function and ρ is a normalization function such as *softmax*

(mask block is optional). The scalar attention layer computes the scalar product between features transformed by φ and ψ and uses the output as an attention weight for aggregating features transformed by α .

Differently, in vector attention, attention weights are vectors that can modulate individual feature channels:

$$\mathbf{y}_i = \sum_{\mathbf{x}_j \in \mathcal{X}} \rho(\gamma(\beta(\varphi(\mathbf{x}_i), \psi(\mathbf{x}_j)) + \delta)) \odot \alpha(\mathbf{x}_j) \quad (9)$$

where β is a relation function (e.g., subtraction) and γ is a mapping function (e.g. an MLP) that produces attention vectors for feature aggregation, \odot is element-wise product.

Both scalar attention and vector attention do not perfectly satisfy our requirements. First, both of them employ position encoding to indicate the absolute position of the input token but we only need a relative relationship. Second, the value is only a derivative of \mathbf{x}_j but we hope it can reflect the relative relationship between \mathbf{x}_i and \mathbf{x}_j as well.

3.2.2 Multi-view Fusing Transformer

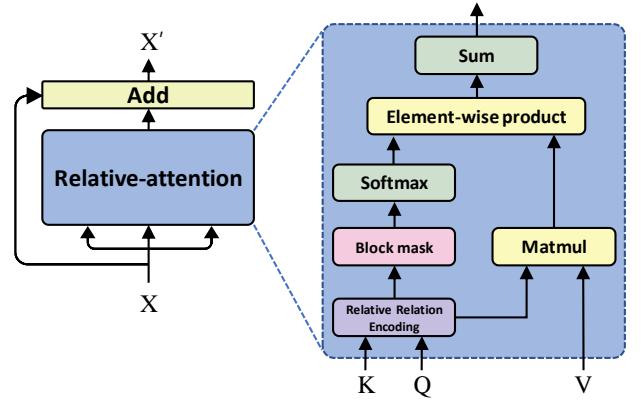


Fig. 4. The architecture of Multi-view Fusing Transformer

To bridge the gap between our purpose and existing transformer models, we propose Multi-view Fusing Transformer (MFT). As shown in Fig. 4 Taking $\mathbf{X} \in \mathbb{R}^{C \times N \times T}$ as input, MFT considers it as the input tokens of $\mathcal{X} = \{\mathbf{x}_i\}_{i=1}^N$, from the perspective of view. The dimension of T is omitted here as the Relative-Attention is equally operated in each time slice. In addition, the dimension of C is divided into K groups so we get $\mathbf{x}_i \in \mathbb{R}^{D \times K}$, $C = D \times K$. The output of MFT is \mathbf{X}' :

$$\mathbf{X}' = \text{RA}(\mathbf{X}) + \mathbf{X} \quad (10)$$

where RA represents Relative-Attention.

In Relative-Attention, the input \mathcal{X} triplicates the role of query, key, and value, the output is $\mathcal{Y} = \{\mathbf{y}_i\}_{i=1}^N$.

$$\mathbf{A}_{ij} = \gamma(\mathfrak{R}(\mathbf{x}_i, \mathbf{x}_j)) \quad (11)$$

$$\mathbf{T}_{ij} = \alpha(\mathfrak{R}(\mathbf{x}_i, \mathbf{x}_j)) \quad (12)$$

$$\mathbf{y}_i = \sum_{\mathbf{x}_j \in \mathcal{X}} \rho(\mathbf{A}_{ij} \odot (\mathbf{T}_{ij} \mathbf{x}_j)) \quad (13)$$

where $\mathfrak{R}(\mathbf{x}_i, \mathbf{x}_j)$ measures the relationship between each pair of view $\{\mathbf{x}_i, \mathbf{x}_j\}$, γ and α further transform $\mathfrak{R}(\mathbf{x}_i, \mathbf{x}_j)$ into attention matrix $\mathbf{A}_{ij} \in \mathbb{R}^{D \times K}$ and transform matrix $\mathbf{T}_{ij} \in \mathbb{R}^{D \times D}$ via fully connected layers, ρ consists of a block mask module and a *softmax*. The block mask module randomly sets all the values

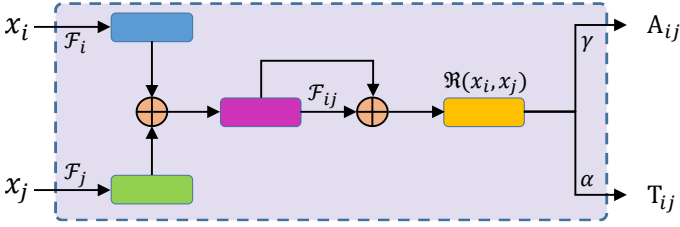


Fig. 5. The architecture of relative relation encoding module

in A_{ij} to $-\infty$ at the rate of M , except diagonal elements, those values are turned into zero after softmax . This mechanism ensures the MFT generalizes well to the scene with an arbitrary number of views. The architecture of $\mathfrak{R}(x_i, x_j)$ is shown in Fig.5, formulated as:

$$\mathfrak{R}(x_i, x_j) = \mathcal{F}_i(x_i) + \mathcal{F}_j(x_j) + \mathcal{F}_{ij}(\mathcal{F}_i(x_i) + \mathcal{F}_j(x_j)) \quad (14)$$

where \mathcal{F}_i , \mathcal{F}_j and \mathcal{F}_{ij} are fully connected layers.

The relative-attention is a vector product-like operation. The difference between them lies in that (1) the explicit position encoding is discarded in query and value items, (2) the relative relationship is also integrated into the value item. In brief, MFT reconstructs the feature of each view according to the relationship between them, formulated as: $\mathbf{X} \rightarrow \mathbf{X}', \mathbf{X}' \in \mathbb{R}^{C \times N \times T}$.

3.3 Temporal Fusing Transformer

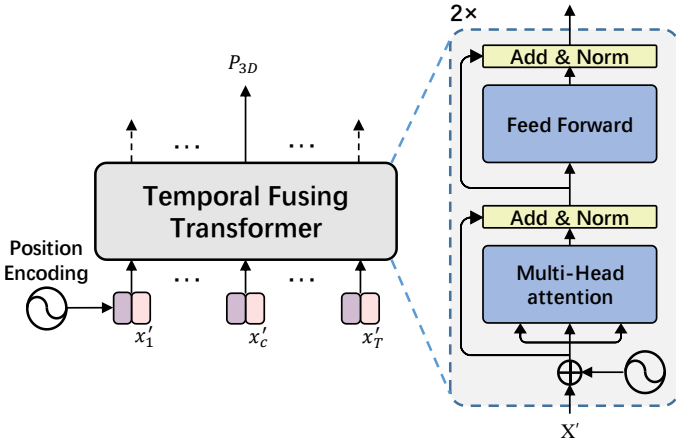


Fig. 6. The architecture of Temporal Fusing Transformer

The Temporal Fusing Transformer (TFT) is shown in Fig. 6, it takes \mathbf{X}' as input and predicts the 3D pose of J joint points $P_{3D} \in \mathbb{R}^{3 \times J \times N}$ in static scenes or dynamic scenes. Specifically, TFT utilizes a Transformer Encoder block [22] of two encoder layers to get the 3D pose of the middle frame. As the temporal sequence has a direction and the order of frames matters, the position encoding is employed here. In addition, TFT masks some frames during the training stage to be compatible with a single image in static scenes and multi-view videos in dynamic scenes. For example, when the input video sequence has 7 frames, the left and right frames are masked evenly.

3.4 Implementation Details

MTF-Transformer is an end-to-end method. We employ pretrained CPN [39] as the 2D detector, and its weights are frozen in the

training stage. We use mean per joint position error (MPJPE) as the loss function and test metric. MPJPE first aligns the root joint(central hip) and then calculates the average Euclidean distance of the estimated joints between the predicted 3D pose and the ground truth. MTF-Transformer is implemented with Pytorch [43]. During the training phase, batch size, learning rate, learning decay, and dropout rate are set to 720, $1e^{-3}$, 0.95, 0.1 respectively. Note that learning decay is executed after the end of every epoch. We adopt the same strategy for BN momentum decay as in [13]. Adam Optimizer [44] is used for all modules. The channel C is 600. The model is trained with 60 epochs on three Pascal TITAN X GPUs.

4 EXPERIMENTS

4.1 Datasets

We evaluate MTF-Transformer on three datasets, including:

Human3.6M (H36M) [24] is a large publicly available 3D human pose benchmark for both monocular and multi-view setups. It consists of 3.6 million image frames from 4 synchronized 50Hz digital cameras and the corresponding 2D pose and 3D pose are captured by the MoCap system in a constrained indoor studio environment. Each actor performs 15 everyday activities such as walking, discussing, etc. Following previous works [9], [51], [52], we use 5 subjects (S1, S5, S6, S7, S8) for training and 2 subjects (S9, S11) for testing, and report MPJPE [13], [14], [34] as the evaluation metric. For a fair comparison, we simulate a virtual view via random rotation and translation, following Cheng et al. [33]. The corresponding 2D pose of the virtual camera is generated via perspective projection.

TotalCapture [25] is captured from 8 calibrated full HD video cameras recording at 60Hz. It features five subjects, each subject performs four diverse performances 3 times, involving ROM, Walking, Acting, and Freestyle. Accurate 3D human joint locations are obtained from a marker-based motion capture system. Following previous work, the training set consists of “ROM1,2,3”, “Walking1,3”, “Freestyle1,2”, “Acting1,2”, on subjects 1,2, and 3. The test set consists of “Walking2 (W2)”, “Freestyle3 (FS3)”, and “Acting3 (A3)” on subjects 1, 2, 3, 4, and 5. The number following each action indicates the video from which the action is. For example, Freestyle has three videos of the same action, of which, 1 and 2 are used for training and 3 for testing. The camera 1,3,5,7 is used in both training and testing set but camera 2,3,6,8 only appear in the testing set. That is to say, the testing set has some unseen camera configuration.

KTH Multiview Football II [26] consists of 8000+ images of professional footballers during a match in the Allsvenskan league. It is filmed by moving cameras and contains 14 joints(top-head, neck, shoulders, hips, knees, feet, elbows, and hands). To match the topology of H36M, we create the root(pelvis) by averaging the hips, the nose by averaging the neck and top-head, and the spine by averaging the root and the neck.

4.2 Quantitative Evaluation

We report the quantitative results of MTF-Transformer on Human3.6M and TotalCapture:

Human3.6M: The quantitative results of MTF-Transformer and competitive methods are shown in Tab. 1. MTF-Transformer outperforms all the monocular methods and MTF-Transformer decreases the MPJPE by 0.9 when increasing the length of sequence from 1 to 7, indicating that temporal information benefits

TABLE 1
Quantitative results on Human3.6M, where M denotes mask rate and T is the length of the sequence. Best results in bold.

	Dir.	Disc.	Eat	Greet	Phone	Photo	Pose	Purch.	Sit	SitD.	Smoke	Wait	WalkD.	Walk	WalkT.	Avg
Monocular methods																
Pavlo et al. [13]	45.2	46.7	43.3	45.6	48.1	55.1	44.6	44.3	57.3	65.8	47.1	44.0	49.0	32.8	33.9	46.8
Chen et al. [45]	43.8	48.6	49.1	49.8	57.6	61.5	45.9	48.3	62.0	73.4	54.8	50.6	56.0	43.4	45.5	52.7
Liu et al. [46]	41.8	44.8	41.1	44.9	47.4	54.1	43.4	42.2	56.2	63.6	45.3	43.5	45.3	31.3	32.2	45.1
Wang et al. [15]	40.2	42.5	42.6	41.1	46.7	56.7	41.4	42.3	56.2	60.4	46.3	42.2	46.2	31.7	31.0	44.5
Zeng et al. [47]	46.6	47.1	43.9	41.6	45.8	49.6	46.5	40.0	53.4	61.1	46.1	42.6	43.1	31.5	32.6	44.8
Multi-view methods with camera parameters																
Pavlakos et al. [48]	41.2	49.2	42.8	43.4	55.6	46.9	40.3	63.7	97.6	119.0	52.1	42.7	51.9	41.8	39.4	56.9
Qiu et al. [36]	24.0	26.7	23.2	24.3	24.8	22.8	24.1	28.6	32.1	26.9	31.0	25.6	25.0	28.0	24.4	26.2
Iskakov et al. [19]	19.9	20.0	18.9	18.5	20.5	19.4	18.4	22.1	22.5	28.7	21.2	20.8	19.7	22.1	20.2	20.8
He et al. [18]	25.7	27.7	23.7	24.8	26.9	31.4	24.9	26.5	28.8	31.7	28.2	26.4	23.6	28.3	23.5	26.9
Zhang et al. [49]	-	-	-	-	-	-	-	-	-	-	-	-	-	-	-	21.7
Remelli et al. [50]	27.3	32.1	25.0	26.5	29.3	35.4	28.8	31.6	36.4	31.7	31.2	29.9	26.9	33.7	30.4	30.2
Multi-view methods without camera parameters																
Huang et al. [21]	26.8	32.0	25.6	52.1	33.3	42.3	25.8	25.9	40.5	76.6	39.1	54.5	35.9	25.1	24.2	37.5
Gordon et al. [38]	23.1	28.8	26.8	28.1	31.6	37.1	25.7	31.4	36.5	39.6	35.0	29.5	35.6	26.8	26.4	30.9
(based on Iskakov et al. [19])	-	-	-	-	-	-	-	-	-	-	-	-	-	-	-	31.7
Gordon et al. [38]	-	-	-	-	-	-	-	-	-	-	-	-	-	-	-	21.7
MTF-Transformer($M=0.4, T=1$)	25.2	29.0	26.9	27.4	30.7	33.2	27.0	27.0	34.3	40.9	29.2	27.0	32.0	25.5	25.9	29.4
MTF-Transformer($M=0.4, T=7$)	24.6	28.3	26.0	26.5	30.0	32.1	26.0	26.3	33.5	39.7	28.4	26.4	31.1	24.6	24.9	28.5

TABLE 2
Quantitative results on TotalCapture, where M denotes mask rate and T is the length of the sequence. * indicates using ground truth 2D pose.

Methods	Seen Cameras(1,3,5,7)							Mean	Unseen Cameras(2,4,6,8)							Mean
	Seen Subjects(S1, S2, S3)			Unseen Subjects(S4, S5)					Seen Subjects(S1, S2, S3)			Unseen Subjects(S4, S5)				
	W2	FS3	A3	W2	FS3	A3		W2	FS3	A3	W2	FS3	A3			
Qiu et al. [36]	19	28	21	32	54	33	29	-	-	-	-	-	-	-		
Remeli et al. [50]	10.6	30.4	16.3	27.0	65.0	34.2	27.5	22.4	47.1	27.8	39.1	75.7	43.1	38.2		
Ours($M = 0.4, T = 1$)*	9.7	24.9	12.6	22.7	42.9	28.9	21.5	17.9	34.7	21.2	29.4	49.3	37.0	29.7		
Ours($M = 0.4, T = 7$)*	9.1	24.0	11.9	22.4	42.4	28.5	21.0	17.5	33.9	20.7	29.2	48.7	36.5	29.2		

for 3D pose estimation. Compared to Multi-view methods with calibration, MTF-Transformer is superior to [48] and [50] but inferior to others. It shows that MTF-Transformer is competitive but camera calibration still has an obvious advantage. Compared to Multi-view methods without calibration, MTF-Transformer achieves the best performance and demonstrates its superiority. Besides, considering the difficulty to calibrate the camera in real-time, MTF-Transformer is a satisfactory attempt.

TotalCapture: The quantitative results of MTF-Transformer and competitive methods are shown in Tab. 2. MTF-Transformer is trained on camera 1, 3, 5, 7 of the training set, and tested on camera 1, 3, 5, 7 (seen) and camera 2, 4, 6, 8 (unseen) of the testing set. Besides, the testing set includes both seen subjects and unseen subjects in the training set. From the vertical comparison, MTF-Transformer outperforms [36] and [50] in all the items and it decreases the MPJPE when changing the length from 1 to 7. It demonstrates the superior of MTF-Transformer and the effect of temporal information. From horizontal analysis, all the methods achieve better performance on seen cameras than on unseen cameras, on seen subjects than on unseen subjects. It means that generalization is an important issue for 3D pose estimation.

4.3 Qualitative Evaluation

Some results of MTF-Transformer on Human3.6M are shown in Fig. 7. When more views participate in the 3D pose estimation, MTF-Transformer obtains better prediction. To further verify the generalization of MTF-Transformer under different camera configurations, we test the model trained on Human3.6M on

more challenging KTH Multiview Football II. Some results of generalization experiments are shown in Fig. 8. It demonstrates that MTF-Transformer can generalize well from indoor lab scene to in the wild environment because it stands free from camera parameters and measures the implicit relationship between views adaptively.

4.4 Ablation Study

In this section, we verify the effectiveness of all modules of MTF-Transformer on Human3.6M. To eliminate the effect of the 2D detector, we take 2D detection from CPN [39] as input.

4.4.1 Analysis on Random Block Mask

Random Block Mask is designed to ensure the generalization ability of MTF-Transformer. To verify the effectiveness of the Random Block Mask module, we train MTF-Transformer on Human3.6M training set with 5 views and set the mask rate M at 0, 0.2, 0.4, 0.6, 0.8, 1 respectively. With M increasing, more features from different views are dropped in the training stage. $M = 0$ indicates that all the views participate in the feature fusing among all the views, and $M = 1$ indicates that each view only fuses with itself. In the testing stage, we test the MTF-Transformer counterparts with different mask rates via feeding testing samples with a different number of views (including 1, 2, 3, and 4 views). The results are shown in Tab. 3. From the vertical comparison, at most mask rates, the performance of MTF-Transformer gets better as the number of views increases, except for the mask rate of 1. When the mask rate is set at 1, the MFT

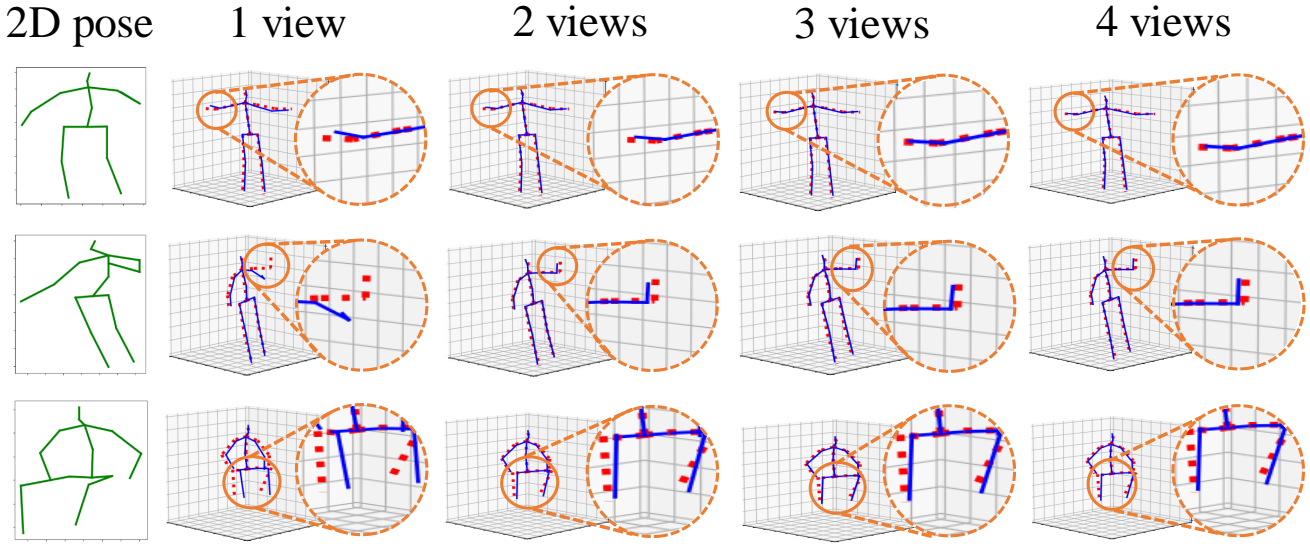


Fig. 7. The result of MTF-Transformer with different view numbers on the Human3.6M. The red dashed line represents GT 3D pose, and the blue solid line represents the predicted 3D pose.

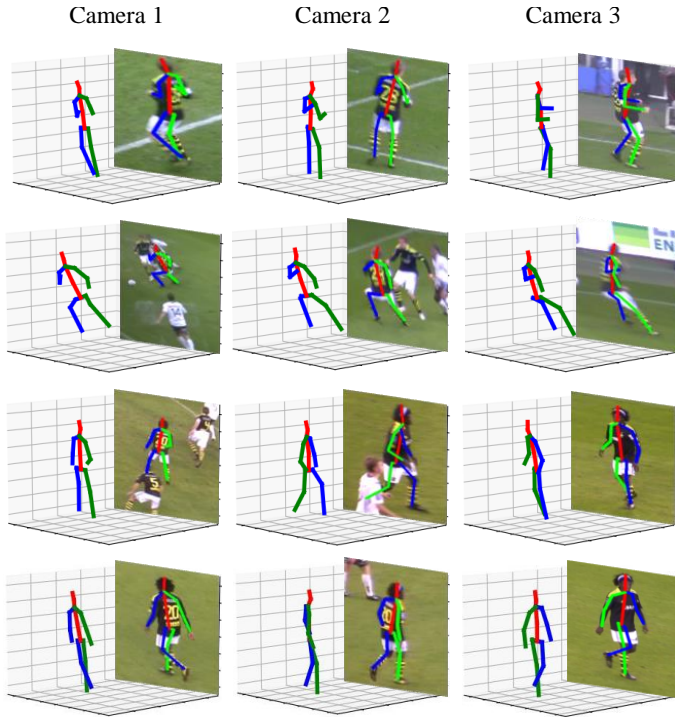


Fig. 8. Demonstration of successful transfer of MTF-Transformer trained on Human3.6M dataset to KTH Multiview Football II scenes.

module fails to measure the relationship among the features since all the interconnections are masked. It verifies that fusing multi-view features can improve the performance of 3D pose estimation. From horizontal analysis, when the number of views is set at 4, MTF-Transformer achieves the best performance at the mask rate of 0 since this number of views in the testing stage is close to that of the training stage (5 views). As the number of views for testing decreases, the difference between training and testing is enlarged and MTF-Transformer achieves the best performance at a higher mask rate. It demonstrates that the Random Block Mask module is essential for scenes that are greatly different from the training

TABLE 3

Results of different mask rate M on Human3.6M. MTF-Transformer is trained on the training set with 5 views at different mask rate. We evaluate these models with different number of views as input.

Mask rate M	0	0.2	0.4	0.6	0.8	1	
Number of views N	1	357.2	53.2	49.4	48.7	48.8	50.3
	2	138.1	35.4	35.2	35.6	38.6	80.1
	3	54.5	29.8	30.4	31.2	35.0	83.4
	4	26.6	27.7	28.5	29.4	33.5	85.4
Mean	144.1	36.5	35.9	36.2	39.0	74.8	

stage. The purpose of MFT-Transformer is to adaptively handle the input from an arbitrary number of views so we evaluate the mean value of the MPJPE at different mask rates. We find that the mask rate of 0.4 has the best result and we will set the mask rate at 0.4 in the following ablation study.

4.4.2 Analysis on Sequence Length

MTF-Transformer can adaptively handle videos with different sequence length. We evaluate it via feeding videos with the length of 1, 3, 5, 7 respectively. The results are shown in Tab. 4. It demonstrates that the performance of MTF-Transformer increases as the sequence length increases, at any number of views as input. Besides, MTF-Transformer can handle the videos of varying sequence length with the same amount of parameters at 10.1M.

4.4.3 Analysis on Confidence Attentive Aggregation

MTF-Transformer employs the Confidence Attentive Aggregation (CAA) module in Feature Extractor to reduce the impact of the unreliable 2D pose. We report the results of MTF-Transformer with and without CAA. Besides, we also evaluate the technique of concatenating the 2D pose and confidence values. As shown in Tab. 5, concatenating can improve the performance, compared with the circumstance without confidence. When CAA takes the place of concatenating, MTF-Transformer can achieve better performance at all the number of views.

TABLE 4
Results of different sequence length T on Human3.6M.

Sequence length T	1	3	5	7	
	1	50.7	49.9	49.6	49.4
Number of views N	2	36.3	35.6	35.4	35.2
	3	31.4	30.8	30.6	30.4
	4	29.4	28.8	28.6	28.5
Parameters(M)	10.1				

TABLE 5
Results of different procedures to fuse the 2D pose and the confidence from 2D detector on Human3.6M.

	Sequence length T	Number of views N				Parameters(M)
		1	2	3	4	
no confidence concatenate CAA	1	52.1	38.1	33.1	31.0	9.8
		51.5	37.8	32.9	30.9	9.8
		50.7	36.3	31.4	29.4	10.1
no confidence concatenate CAA	3	51.1	37.1	32.2	30.2	9.8
		50.7	36.9	32.1	30.2	9.8
		49.9	35.6	30.8	28.8	10.1
no confidence concatenate CAA	5	50.7	36.8	31.9	29.9	9.8
		50.3	36.6	31.8	29.9	9.8
		49.6	35.4	30.6	28.6	10.1
no confidence concatenate CAA	7	50.5	36.6	31.7	29.8	9.8
		50.1	36.4	31.6	29.8	9.8
		49.4	35.2	30.4	28.5	10.1

4.4.4 Analysis on Multi-view Fusing Transformer

The Multi-view Fusing Transformer (MFT) measures the relationship between each pair of views and reconstructs the features according to the relationship. To validate the effectiveness of MFT, we first validate the results of MTF-Transformer on Human3.6M with and without MFT. Then, we validate the design of Relation-attention.

When the MFT is not employed, the MTF-Transformer degrade to deal with each view individually so it has the same result regardless of the number of views. We train MTF-Transformer on the training set and test it on seen cameras (0,2), unseen cameras (1,3), and all cameras (1,2,3,4) on the testing set. As shown in Tab. 8, MFT can improve the performance of MTF-Transformer on seen, unseen, and all cameras with the most number of views, except 1 view. This is because that MTF-Transformer without MFT always deals with input with 1 view, there is no generalization gap between the training and testing stage. However, when the number of views increases, the MTF-Transformer without MFT is worse.

In the Relative-attention module, we intergrade the relationship between each pair of views into the value of the attention mechanism. To validate the effectiveness of the transform matrix T_{ij} , we remove it from the relative-attention module. As shown in Tab. 6, the transform matrix improves the performance at most number of views except 1 view, because the MFT fuse the feature with itself when only 1 view is used.

4.4.5 Analysis on computational complexity

As shown in Tab. 4.4.5, we report the total number of parameters and estimated multiply-add operations (MACs) per frame. For

TABLE 6
Results of different design of Relative Position Encoding on Human3.6M.

	Sequence length T	Number of views N				Parameters(M)
		1	2	3	4	
with T_{ij} without T_{ij}	1	50.7	36.3	31.4	29.4	10.1
		50.3	38.4	33.4	31.1	9.7
with T_{ij} without T_{ij}	3	49.9	35.6	30.8	28.8	10.1
		49.5	37.4	32.5	30.3	9.7
with T_{ij} without T_{ij}	5	49.6	35.4	30.6	28.6	10.1
		49.3	37.1	32.2	30.0	9.7
with T_{ij} without T_{ij}	7	49.4	35.2	30.4	28.5	10.1
		49.0	36.9	32.0	29.8	9.7

TABLE 7
Computational complexity of MTF-Transformer. We use THOP¹ to represent the number of parameters and MACs (multiply-add operations).

	Temporal length T	Number of views N	Parameters(M)	MACs(G)
V2V [19]	1	4	11.9	155
MTF-Transformer	1	1	10.1	0.01
		2		0.03
		3		0.05
		4		0.07
	2	1	10.1	0.03
		2		0.08
		3		0.10
		4		0.2
	3	1	10.1	0.05
		2		0.10
		3		0.20
		4		0.40
4	1	10.1	0.07	
	2		0.20	
	3		0.30	
	4		0.50	

comparison, we also report parameters and MACs of V2V [19]. Similar to MTF-Transformer, V2V also infers the 3D pose via lifting multi-view 2D detections to 3D detections. MTF-Transformer has a slightly less number of parameters and orders of magnitude less computational complexity than V2V. The reason is that MTF-Transformer employs 1D convolution to manipulate the features, instead of 3D convolution.

5 CONCLUSION

We present a unified framework MTF-Transformer to fuse multi-view sequences in uncalibrated scenes with an arbitrary number of views. MTF-Transformer can adaptively measure the relationship between each pair of views with a relative-attention mechanism, avoiding the dependency on camera calibration. It is also computationally lightweight and can be directly applied to settings where the number of views and video frames varies. Extensive experimental results demonstrate the effectiveness and robustness of the MTF-Transformer.

1. github.com/Lyken17/pytorch-OpCounter

TABLE 8
Results of with and without MFT module on Human3.6M.

	Sequence length T	seen cameras(0,2)		unseen cameras(1,3)		all cameras(0,1,2,3)				Parameters(M)
		1	2	1	2	1	2	3	4	
without MFT	1		51.8		62.1		56.9			7.5
with MFT		52.1	37.1	62.1	47.2	57.1	46.9	42.4	40.0	10.1
without MFT	3		51.0		61.4		56.2			7.5
with MFT		51.2	36.3	61.4	46.4	56.3	46.0	41.6	39.1	10.1
without MFT	5		50.8		61.2		56.0			7.5
with MFT		50.9	36.0	61.2	46.2	56.1	45.8	41.3	38.9	10.1
without MFT	7		50.6		60.9		55.7			7.5
with MFT		50.8	35.8	61.0	46.0	55.9	45.6	41.2	38.8	10.1

REFERENCES

- [1] J. Carreira and A. Zisserman, "Quo vadis, action recognition? a new model and the kinetics dataset," *IEEE Computer Society*, 2017. **1**
- [2] J. Liu, W. Gang, H. Ping, L. Y. Duan, and A. C. Kot, "Global context-aware attention lstm networks for 3d action recognition," in *IEEE Conference on Computer Vision & Pattern Recognition*, 2017. **1**
- [3] D. C. Luvizon, D. Picard, and H. Tabia, "2d/3d pose estimation and action recognition using multitask deep learning," in *2018 IEEE/CVF Conference on Computer Vision and Pattern Recognition*, 2018. **1**
- [4] —, "2d/3d pose estimation and action recognition using multitask deep learning," in *2018 IEEE/CVF Conference on Computer Vision and Pattern Recognition*, 2018. **1**
- [5] A. Kanazawa, M. J. Black, D. W. Jacobs, and J. Malik, "End-to-end recovery of human shape and pose," *IEEE*, 2018. **1, 2**
- [6] A. S. Jackson, C. Manafas, and G. Tzimiropoulos, "3d human body reconstruction from a single image via volumetric regression," *European Conference on Computer Vision*, 2018. **1**
- [7] B. M. Smith, V. Chari, A. Agrawal, J. M. Rehg, and R. Sever, "Towards accurate 3d human body reconstruction from silhouettes," in *2019 International Conference on 3D Vision (3DV)*, 2019. **1**
- [8] X. B. Peng, P. Abbeel, S. Levine, and V. Michiel, "Deepmimic: Example-guided deep reinforcement learning of physics-based character skills," *ACM Transactions on Graphics*, vol. 37, no. 4CD, pp. 143.1–143.14, 2018. **1**
- [9] J. Martinez, R. Hossain, J. Romero, and J. J. Little, "A simple yet effective baseline for 3d human pose estimation," *IEEE*, 2017. **1, 2, 3, 5**
- [10] F. Moreno-Noguer, "3d human pose estimation from a single image via distance matrix regression," 2016. **1**
- [11] S. Sharma, P. T. Varigonda, P. Bindal, A. Sharma, and A. Jain, "Monocular 3d human pose estimation by generation and ordinal ranking," *IEEE*, 2019. **1**
- [12] L. Zhao, X. Peng, Y. Tian, M. Kapadia, and D. N. Metaxas, "Semantic graph convolutional networks for 3d human pose regression," *IEEE*, 2019. **1**
- [13] D. Pavllo, C. Feichtenhofer, D. Grangier, and M. Auli, "3d human pose estimation in video with temporal convolutions and semi-supervised training," 2019. **1, 2, 5, 6**
- [14] Y. Cai, L. Ge, J. Liu, J. Cai, and N. M. Thalmann, "Exploiting spatial-temporal relationships for 3d pose estimation via graph convolutional networks," in *2019 IEEE/CVF International Conference on Computer Vision (ICCV)*, 2019. **1, 2, 5**
- [15] J. Wang, S. Yan, Y. Xiong, and D. Lin, "Motion guided 3d pose estimation from videos," 2020. **1, 2, 6**
- [16] A. Zeng, X. Sun, L. Yang, N. Zhao, M. Liu, and Q. Xu, "Learning skeletal graph neural networks for hard 3d pose estimation," 2021. **1**
- [17] C. Zheng, S. Zhu, M. Mendieta, T. Yang, C. Chen, and Z. Ding, "3d human pose estimation with spatial and temporal transformers," 2021. **1**
- [18] Y. He, R. Yan, K. Fragkiadaki, and S.-I. Yu, "Epipolar transformers," 2020. **1, 2, 6**
- [19] K. Isakov, E. Burkov, V. Lempitsky, and Y. Malkov, "Learnable triangulation of human pose," 2019. **1, 2, 6, 8**
- [20] Z. Zhang, C. Wang, W. Qiu, W. Qin, and W. Zeng, "Adafuse: Adaptive multiview fusion for accurate human pose estimation in the wild," *International Journal of Computer Vision*, vol. 129, no. 3, p. 703–718, Nov 2020. [Online]. Available: <http://dx.doi.org/10.1007/s11263-020-01398-9> **1**
- [21] F. Huang, A. Zeng, M. Liu, Q. Lai, and Q. Xu, "Deepfuse: An imu-aware network for real-time 3d human pose estimation from multi-view image," 2019. **1, 2, 6**
- [22] A. Vaswani, N. Shazeer, N. Parmar, J. Uszkoreit, L. Jones, A. N. Gomez, L. Kaiser, and I. Polosukhin, "Attention is all you need," 2017. **2, 5**
- [23] "Dropout: A simple way to prevent neural networks from overfitting," *Journal of Machine Learning Research*, vol. 15, no. 1, pp. 1929–1958, 2014. **2**
- [24] C. Ionescu, D. Papava, V. Olaru, and C. Sminchisescu, "Human3.6m: Large scale datasets and predictive methods for 3d human sensing in natural environments," *IEEE Transactions on Pattern Analysis & Machine Intelligence*, vol. 36, no. 7, pp. 1325–1339, 2014. **2, 5**
- [25] M. Trumble, A. Gilbert, C. Malleson, A. Hilton, and J. Collomosse, "Total capture: 3d human pose estimation fusing video and inertial sensors," in *2017 British Machine Vision Conference (BMVC)*, 2017. **2, 5**
- [26] V. Kazemi, M. Burenius, H. Azizpour, and J. Sullivan, "Multi-view body part recognition with random forests," in *British Machine Vision Conference*, 2013. **2, 5**
- [27] X. Sun, B. Xiao, F. Wei, S. Liang, and Y. Wei, "Integral human pose regression," 2018. **2**
- [28] G. Pavlakos, X. Zhou, K. G. Derpanis, and K. Daniilidis, "Coarse-to-fine volumetric prediction for single-image 3d human pose," *IEEE Computer Society*, 2016. **2**
- [29] K. Zhou, X. Han, N. Jiang, K. Jia, and J. Lu, "Hemlets pose: Learning part-centric heatmap triplets for accurate 3d human pose estimation," 2019. **2**
- [30] S. Li and A. B. Chan, "3d human pose estimation from monocular images with deep convolutional neural network," *Springer International Publishing*, 2014. **2**
- [31] Z. Wang, D. Shin, and C. C. Fowlkes, "Predicting camera viewpoint improves cross-dataset generalization for 3d human pose estimation," 2020. **2**
- [32] S. Li, L. Ke, K. Pratama, Y.-W. Tai, C.-K. Tang, and K.-T. Cheng, "Cascaded deep monocular 3d human pose estimation with evolutionary training data," *2020 IEEE/CVF Conference on Computer Vision and Pattern Recognition (CVPR)*, Jun 2020. [Online]. Available: <http://dx.doi.org/10.1109/CVPR42600.2020.00621> **2**
- [33] Y. Cheng, B. Yang, B. Wang, Y. Wending, and R. Tan, "Occlusion-aware networks for 3d human pose estimation in video," in *2019 IEEE/CVF International Conference on Computer Vision (ICCV)*, 2019, pp. 723–732. **2, 5**
- [34] J. Lin and G. H. Lee, "Trajectory space factorization for deep video-based 3d human pose estimation," 2019. **2, 5**
- [35] J. Dong, W. Jiang, Q. Huang, H. Bao, and X. Zhou, "Fast and robust multi-person 3d pose estimation from multiple views," 2019. **2**
- [36] H. Qiu, C. Wang, J. Wang, N. Wang, and W. Zeng, "Cross view fusion for 3d human pose estimation," 2019. **2, 6**
- [37] A. Kadhodamohammadi and N. Padoy, "A generalizable approach for multi-view 3d human pose regression," 2019. **2**
- [38] B. Gordon, S. Raab, G. Azov, R. Giryes, and D. Cohen-Or, "Flex: Parameter-free multi-view 3d human motion reconstruction," 2021. **2, 3, 6**
- [39] Y. Chen, Z. Wang, Y. Peng, Z. Zhang, G. Yu, and J. Sun, "Cascaded pyramid network for multi-person pose estimation." **3, 5, 6**
- [40] M. Raghu, T. Unterthiner, S. Kornblith, C. Zhang, and A. Dosovitskiy, "Do vision transformers see like convolutional neural networks?" *arXiv preprint arXiv:2108.08810*, 2021. **4**

- [41] A. Vaswani, N. Shazeer, N. Parmar, J. Uszkoreit, L. Jones, A. N. Gomez, Ł. Kaiser, and I. Polosukhin, "Attention is all you need," in *Advances in neural information processing systems*, 2017, pp. 5998–6008. 4
- [42] H. Zhao, L. Jiang, J. Jia, P. H. Torr, and V. Koltun, "Point transformer," in *Proceedings of the IEEE/CVF International Conference on Computer Vision*, 2021, pp. 16259–16268. 4
- [43] A. Paszke, S. Gross, S. Chintala, G. Chanan, E. Yang, Z. Devito, Z. Lin, A. Desmaison, L. Antiga, and A. Lerer, "Automatic differentiation in pytorch," 2017. 5
- [44] D. Kingma and J. Ba, "Adam: A method for stochastic optimization," *Computer Science*, 2014. 5
- [45] C. Li and G. H. Lee, "Generating multiple hypotheses for 3d human pose estimation with mixture density network," 2019. 6
- [46] R. Liu, J. Shen, H. Wang, C. Chen, and V. Asari, "Attention mechanism exploits temporal contexts: Real-time 3d human pose reconstruction," in *2020 IEEE/CVF Conference on Computer Vision and Pattern Recognition (CVPR)*, 2020. 6
- [47] A. Zeng, X. Sun, F. Huang, M. Liu, Q. Xu, and S. Lin, "Srnet: Improving generalization in 3d human pose estimation with a split-and-recombine approach," 2020. 6
- [48] G. Pavlakos, X. Zhou, K. G. Derpanis, and K. Daniilidis, "Harvesting multiple views for marker-less 3d human pose annotations," 2017. 6
- [49] Z. Zhang, C. Wang, W. Qin, and W. Zeng, "Fusing wearable imus with multi-view images for human pose estimation: A geometric approach," 2020. 6
- [50] E. Remelli, S. Han, S. Honari, P. Fua, and R. Wang, "Lightweight multi-view 3d pose estimation through camera-disentangled representation," 2020. 6
- [51] K. Lee, I. Lee, and S. Lee, "Propagating lstm: 3d pose estimation based on joint interdependency," *Springer, Cham*, 2018. 5
- [52] X. Sun, J. Shang, S. Liang, and Y. Wei, "Compositional human pose regression," *Computer Vision and Image Understanding*, 2017. 5



Hui Shuai received the M.S degree from Nanjing University of Information Science and Technology (NUIST) in 2018. He is currently working toward the PhD degree with NUIST. His current research interests include object detection and 3D point cloud analysis.



Lele Wu received the bachelor's degree from the Nanjing University of Information Science and Technology (NUIST) in 2019, where he is currently pursuing the master's degree. His research interests include 3D human pose estimation and computer vision.



Qingshan Liu (M'05–SM'07) received the M.S. degree from Southeast University, Nanjing, China, in 2000 and the Ph.D. degree from the Chinese Academy of Sciences, Beijing, China, in 2003. He is currently a Professor in the School of Computer and Software, Nanjing University of Information Science and Technology, Nanjing. His research interests include pattern recognition, image and video analysis.